VĚDECKÉ SPISY VYSOKÉHO UČENÍ TECHNICKÉHO V BRNĚ

Edice PhD Thesis, sv. 699

ISSN 1213-4198

Ing. Alexandr Knápek

Methods of Preparation and Characterisation of Experimental Field-Emission Cathodes

VYSOKÉ UČENÍ TECHNICKÉ V BRNĚ
Fakulta elektrotechniky a komunikačních technologií
Ústav fyziky

Ing. Alexandr Knápek

METHODS OF PREPARATION AND CHARACTERISATION OF EXPERIMENTAL FIELD-EMISSION CATHODES

METODY PŘÍPRAVY A CHARAKTERIZACE EXPERIMENTÁLNÍCH AUTOEMISNÍCH KATOD

Zkrácená verze Ph.D. Thesis

Obor: Fyzikální elektronika a nanotechnologie
Školitel: prof. Ing. Lubomír Grmela, CSc.
Oponenti: doc. Ing. Josef Lazar, Ph.D.
prof. Dr. RNDr. Jiří Luňáček
Datum obhajoby: 11. 4. 2013

Klíčová slova

Autoemisní katoda, šumová spektroskopie.

Key words

Field-emission cathode, noise spectroscopy.

Místo uložení práce

Práce je k dispozici na Vědeckém oddělení děkanátu Fakulty Elektrotechniky a komunikačních technologií VUT v Brně, Technická 10, Brno, 616 00.

ISBN 978-80-214-4728-8
ISSN 1213-4198

CONTENTS

1 INTRODUCTION

Electron devices utilizing a focused electron beam require a high-quality source of free electrons that is sufficiently bright, able to provide high current density, and able to work in low-quality vacuum conditions.

This thesis discusses an experimental emitter that meets all the requirements stated above. However, the stability of the emission must be further described and analysed, since this is considered to be one of the essential parameters determining the quality of an electron beam.

An experimental field-emission emitter based on an ultra sharp emitter with a metal-oxide-dielectric structure proved to be the ideal candidate based on the conditions stated above. This emitter is further examined in order to make it the electron source for a low-energy transmission electron microscope (TEM) that is currently being developed by Delong Instruments. There are several reasons why we find this kind of emitter to be beneficial for use in a new type of "desktop"low-energy TEM.

Regarding the advantages of the cold field-emission sources, it should be emphasized that only slight demagnification is required to obtain a 1-nm-diameter probe, because of the small virtual source (2-5 nm). Secondly, there is only a very small energy spread, which enables operation at low accelerating voltages, which in turns makes it possible to obtain a very sharp, high-contrast image without major radiation damage to the specimen, especially when working with biological specimens (e.g. tissues or single cells).

Lastly, thanks to the epoxy layer, it is possible to work in relatively low-quality vacuum (less than 10^{-6} Pa), preventing the ion-bombardment and chemi/physisorption of residuals on the surface of the tip. The preservation of the lower vacuum also enables faster manipulation with the sample and generally lower price comparing to devices working with UHV (more than 10^{-7} Pa).

As it was mentioned in the opening, these sources are still not stable enough to provide a high-quality source of electrons. Thus it is necessary to examine and improve preparation procedures so as to minimize current fluctuations. New techniques must be found, as well as suitable methods for describing the structure and providing the information needed to perform a further theoretical simulation, which will help us to understand the correlation between the structure and the resulting electron emission.

2 THEORETICAL BASIS

2.1 Scientific Field Development

Researchers' interest in field emission of electrons, a phenomenon known since 1897 [25], dates back to the first half of the twentieth century and is mostly associated with the development of the electron microscope. The development of electron sources was made possible primarily by a work of H. Busch [1], published in 1926, which showed that solenoid deflection systems and magnetic fields could act analogically to classical optical lenses. At the beginning of the 1930s, interest in research on field-emission sources increased slightly, mostly in connection with the electron microscope prototype constructed by a team led by Knoll and Ruska. In years following that, many papers were published that were focused on the properties of field-emission sources. The electron sources of that era consisted mainly of tungsten mono-crystalline tips with various crystallographic orientations [17], [24], [8].

As the development of devices utilizing a focused electron beam progressed, demands on their parameters increased significantly, and so these parameters continuously improved. Electron optical components showed particular improvement. Electron sources became especially popular after 1956, when prof. Hibi, one of the pioneers of electron microscopy, pointed out the beneficial properties of sharp thermionic-cathodes [14]. However, the first projects using purely field-emission based sources did not begin appearing until 1954, the first utilization of the field-emission appeared lately in 1968 as a part of scanning electron microscope [2], [3].

2.2 State of Art

In recent years, further developments in the field of production of field-emission cathodes has been brought. This enabled widespread use of field-emission cathodes. Meanwhile technological advances in the field of vacuum preservation have also been important, since a high-quality vacuum is essential for ensuring reliable field-emission cathodes. In the past three decades, cathode-manufacturing technology based on electrolytic etching [18] has been investigated and enhanced. This technology makes it possible to prepare a cathode tip with a diameter of just a few dozen nanometers, and thus to meet one of the main criteria for a high-quality field-emission source. Along with recent progress in the area of inorganic chemistry and in the field of applied technology disciplines, these are leading to an ongoing broadening of the range of materials used [5], [19], [11].

3 OBJECTIVES OF THIS WORK

The aim of this work is to describe the main mechanisms influencing current instability in field-emission sources and to suggest improvements to cathode fabrication, developing the new method of reproducible cathode preparation. Recent studies have drawn attention to the presence of current fluctuations occurring in the investigated structure, that causes electrical noise on both thermionic and field-emission cathodes [26].

Current research, based on noise spectral density analysis, reveals the presence of relatively large characteristic noise, whose dominant component, called "$1/f$ noise", is easily correlated with flickering of the emission current. This and other types of noise, which are mutually superimposed, has already been described in detail and modeled mathematically [22], [6]. Based on these results, it seems appropriate to use the noise spectrum diagnostic method when diagnosing and describing the field-emission cathodes. This technique enables us to learn about the origin of any transport phenomena taking place during the electron emission.

Exact knowledge of the charge transport behavior is needed in order to analyze the cathode's structure and to suggest technology improvements and conditions to further reduce current fluctuations. Our criteria for materials to be used in the preparation of emission cathodesare: low chemical activity, high melting point, high mechanical strength, and especially the low work function of electrons. And indeed, tungsten has been used from the beginnings of cathode history due to precisely these virtues. However, it is almost impossible to assure an atomically clean tungsten surface, the metal-oxide interface has to be analysed and further taken in the account in the pursuit of our studies.

Last goal of the thesis is connected with theoretical simulations, which are performed using finite element method (FEM), implemented via scientific software Comsol 4.2a. The output of these simulations, based on FEM calculations using Comsol 4.2a, provides basic information about potential distribution near the cathode's tip , allowing us to trace the electrons coming out of the emission plane.

4 ANALYSIS OF THE FIELD EMISSION EMITTER BEHAVIOR

4.1 Characteristics of Material Parameters

The cathode material must satisfy certain criteria in order to ensure cathode functionality. These are: a high melting point, a low work function, large mechanical strength, and a low chemical affinity. Tungsten remains the most widespread cathode material precisely because it meets all of these criteria except for the work function. Tungsten's work function $\varphi = 4.5$ eV is considered to be slightly higher than for other suitable metals (for instance: Ta, at 4.31 eV; or Hf, at 3.9 eV).

4.2 Electron Emitters Based on Field Emission

Field emission sources are generally based on the influence of an external electric field. Temperature does not have significant influence here, although it does slightly help to stabilize the chemical structure at the cathode surface. For field emission cathodes, operating temperatures start from 300 to 1800 K. In general, the work pressures used for field emission sources are lower than for thermoemission sources, and it is necessary to operate these cathodes in high-vacuum conditions ($P \sim 10^{-5}$ to 10^{-6} Pa).

Unlike thermoemission sources, a field emission based electron jet does not need to form a crossover (see fig. 3.3), because a virtual source can be used as well. The emission current is adjusted by setting the voltage on the extractor and suppressor. For jets based on field emission, the cathode temperature is considered to be a fundamental parameter for setting the mode of operation, especially the level of the emission current.

Every field emission source is limited by the level of overall current drawn by the cathode (max. 300 μA). However, this limitation is not a significant problem for micro-analytical purposes, because electron beams with a current stronger than 10^{-6}A can not be focused to under micrometer dimensions.

In order to take advantage of the high electron beam brightness of field emission sources, it is necessary to design a jet with the smallest possible optical aberration. This issue becomes very important when constructing a power field emission jet. Although many experiments have been done with the use of various metals (YB_6, ZrC, TaC...) ungsten remains the most common material. In most cases, a 0.1 or 0.2 mm thick tungsten wire is used to create the electron jet. The classification into a pure field emission or thermionic field emission device depends on the emitter's chemical activity. Emitters with low chemical activity can operate at room temperature. For emitters with higher chemical activity it is necessary to supply thermal energy in order to prevent the

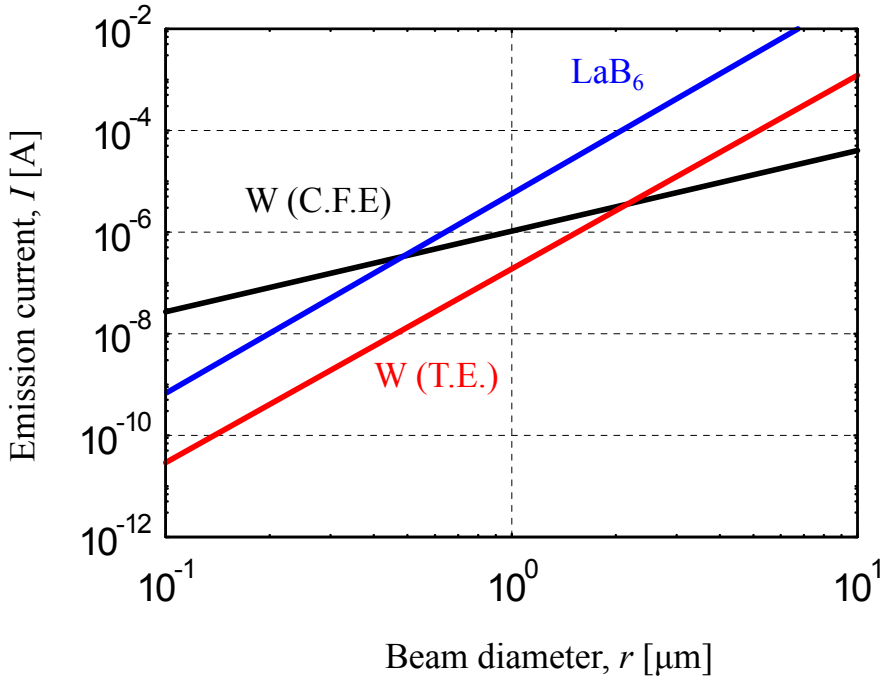

Fig. 4.1: The dependence of the current to the beam diameter for a) LaB_6 source b) thermoemission c) field emission [7].

change to the work function that occurs due to chemi/physisorption of the residual gases on the surface of the emission tip. Tungsten emission tips are usually prepared using electrochemical etching and fixed to the cathode holder using spot welding (hairpin tip cathode) [7], [18].

For field emission jets operating at low temperatures (including those operating at room temperature), the characteristic emission properties of oriented monocrystalline tungsten wires are utilized [2]. Various crystalline planes have various work functions and chemical affinities.

For pure, monocrystalline-based field emission sources, the most suitable configuration is (310), which has the lowest work function and chemical affinity. This means that for cathodes with a structure belonging to that crystalline orientation, the current density will reach its optimal value, and the cathode will be able to work at room temperature (at a high pressure where $P \sim 10^{-8}$ Pa) for a couple of hours with no need of flashing. The highest beam brightness is reached using a special formed emission tip, whose design is influenced by the operating temperature and by the electric field [7]. The typical diameter of the emission tip ranges from 0.05 to 0.1 μm.

The electric field intensity near the cathode surface reaches over 10^9 V $\times$ m^{-1}. Electron beam brightness when operating at a voltage of 25 kV reaches values up to 10^{13} A $\times$ m^{-2} $\times$ sr^{-1}. The first anode, with a variable potential level (2-5 kV), drives the emission current. The second anode is grounded. The work function

determines the cathode potential. Both cathodes can be configured to create either a strong electrostatic lens ensuring beam focusing [3] or a weak lens, which generates a divergent beam requiring further focusing via e.g. a magnetic lens [4]. The two simplest optical arrangements are shown in fig. 4.2.

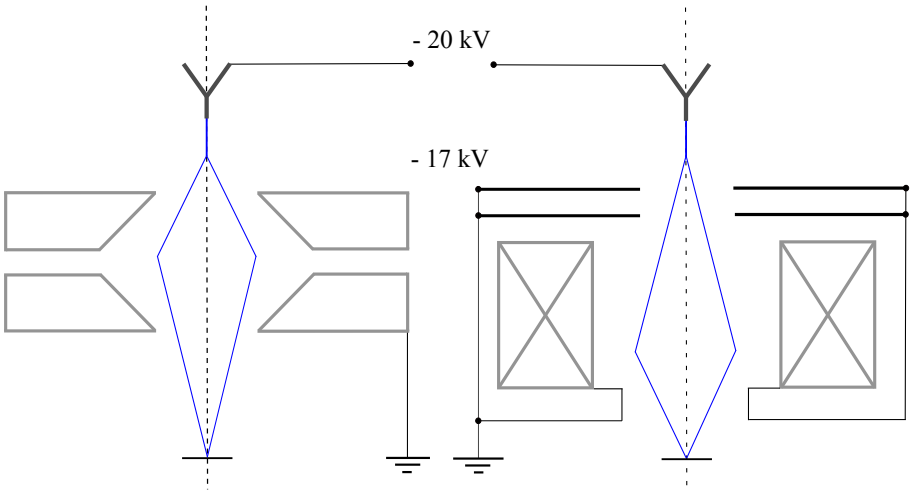

Fig. 4.2: Scheme of the one stage focused configuration with field emission source based on: a) electrostatic projection lens b) magnetic projection lens. [4]

Considering the virtual source's small size (in the single nm), a single-level optical system (of 1 : 1 ratio) is sufficient for most scanning electron microscopy applications, as well as for microanalysis. Field emission sources operating at room temperature have the narrowest energy band (0.1 - 0.2 eV) though they achieve low emission currents (max. 20 μA of the overall current). Tungsten's work function, which is relatively high, is further lowered by adsorption of the molecules and atoms in the residual gases. This process leads to the gradual increase of low-frequency noise. At the same time, the emission current increases until the cathode is eventually destroyed by an electric burst. The cathode therefore must be flashed periodically by heating it to a temperature of 1000 K in order to keep the surface clean. For this very reason field emission cathodes are sometimes operated with slightly increased temperature conditions.

5 EXPERIMENTAL RESULTS

5.1 Preparation Method

For the cathode preparation, polycrystalline-tungsten wire with a diameter of 0.1 mm immersed in a solution of NaOH is generally used. The NaOH solution is present in two molar concentrations (2 and 0.2 mol $\cdot$ dm^{-3}) for the first and second etching phase. Electrochemical polishing is performed in a 0.2 mol $\cdot$ dm^{-3} solution. The moving part of the etching setup consists of a micro-metric stepper-motor-controlled device provides for accurate movement. The static part of the etching setup contains a chemically resistant cylinder in which the electrolyte is located. Laboratory preparation consists of a few basic steps that are described further in the text.

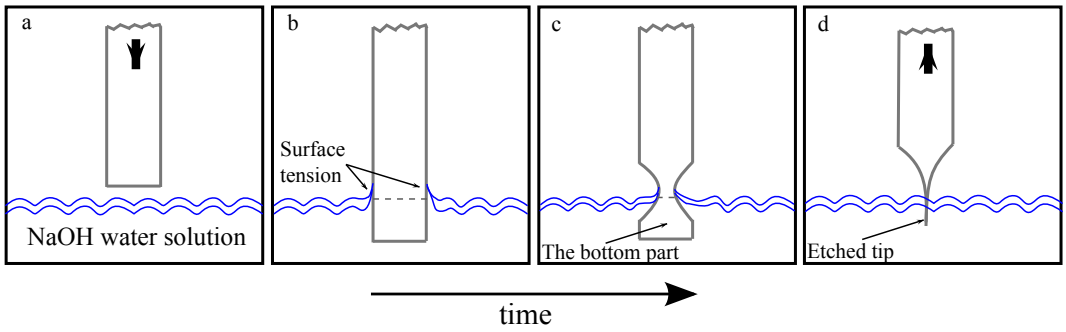

Fig. 5.1: The etching procedure: a) immersing tungsten wire into the electrolyte b) surface tension forming the tip geometry during etching c) the bottom part starts to separate d) the bottom part drops off

1. Step - **mechanical cleaning** - mechanical cleaning - the wire is cleaned using abrasive paper of a high granularity (2000 – 2500 granules/cm^2) removing oxide layers, additive impurities, and carbon particles. Carbon particles occur on the metal surface as residuum arising from the tungsten-wire preparation process. The number of carbon particles can be reduced by using the purest available tungsten wire.
2. Step - **chemical cleaning** - wire is rinsed in hexane dissolves and extracts oily contaminants along fatty acids.
3. Step - **electrochemical cleaning** - after the mechanical and chemical cleaning phases, and before the first etching phase, the wire is polished using an AC current of defined frequency and amplitude, which makes the surface smooth and improves the wire's wettability.

4. Step - **surface detection and wire immersion** - dduring wire immersion, the current value is continually measured, and in the moment when it reaches a defined value, the micro-metric lifter is held in place. Using this method, we can precisely position the wire on the solution surface. 5.1.a
5. Step - **first etching phase** - in this phase, the immersed wire is etched in a 2 M solution of NaOH with DC voltage (6.9 V) applied. The first phase runs until a current threshold is reached (usually around 3.5 mA). After the first phase, the wire gets most thin near the surface, but is still connected to the bottom part. Near the surface, the etching process runs faster; this is due to the surface tension pressing on the tungsten wire. 5.1.b
6. Step - **reset the position of etched wire** - this is the most critical part of the whole preparation process. The constricted region must be set approx 0.2 mm higher against the solution surface. The surface tension directly influences the final shape of the tip apex and is followed by the dropping off of the bottom part. 5.1.c
7. Step - **second etching phase** - in this phase, the final tip shape is prepared. Etching takes place in a 0.2 M NaOH solution with exponentially lowering voltage which is continuously set by the computer. Lowering the voltage lowers the current density before the tip is drawn up out of the solution. 5.1.d
8. Step - **the drop off detection** - during etching, the current values are continually measured and saved at discrete time intervals. The drop off detector, activated when the current approaches a preset current range, immediately starts waiting for the rapid current decrease that occurs just after the bottom part drops off. When the dropping off of the bottom part is detected, the wire must immediately be slid out of the electrolyte, since the wire could become over-etched or additionally contaminated by residuals that are attracted to the etched tip.
9. Step - **additional technological steps** - these steps are executed so as to reach the required clearance and to increase the tip's chemical immunity. Firstly, the tip is immersed in distilled water in order to remove solution residuals. Then the tip is immersed in sulphurous acid, since the acid is a reduction agent and removes hydrocarbon residuals without unwanted oxidization.
10. Step - **epoxy coating** - epoxy coating – finally, the tip is covered in an epoxy coating and placed in a vacuum chamber. The epoxy is polymerized in a special temperature chamber for two different phases.

5.2 Automated Etching System

Our main requirement for the etching setup was that it be a complete and automated system capable of controlling all the necessary processes centrally from a single computer. This means that the system's computer should measure and record physical quantities and also send and receive instrument commands over the GPIB communication interface.

All data needed for preparation is gathered continually during preparation, allows for flexible control of the whole process. The controlling application was completely programmed in MATLAB, which provides for easy implementation and communication with the external instruments (the multimeter, the programmable DC source, and above all the micro-metric lifter) as well as easy modification of the current-etching algorithm.

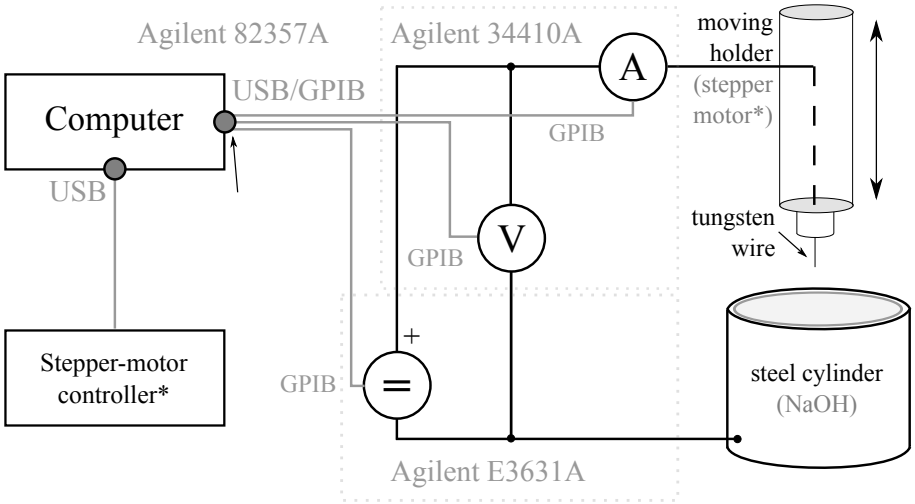

Fig. 5.2: The experimental setup of the electrochemical etching setup.

The whole preparation process is controlled and evaluated by the computer in real time, which enables it to detect the current preparation state at any given instant in time and to respond with appropriate actions based to events as they occur. The zero position of the wire (the position when the wire touches the solution surface) is set with micrometric precision based on the measured conductivity. The core idea behind the system is to trigger the software whenever the etched wire touches the electrolyte's surface, which causes a quick current increase of roughly a few dozen microamperes. This principle is used throughout the preparation process whenever is necessary to lay the bottom part onto the electrolyte surface.

To design a suitable method for controlling the etching current, it is necessary to describe the etching current and understand its behaviour during the pursuit of the wire etching. As mentioned above, the tip etching consists of two phases. The first phase is

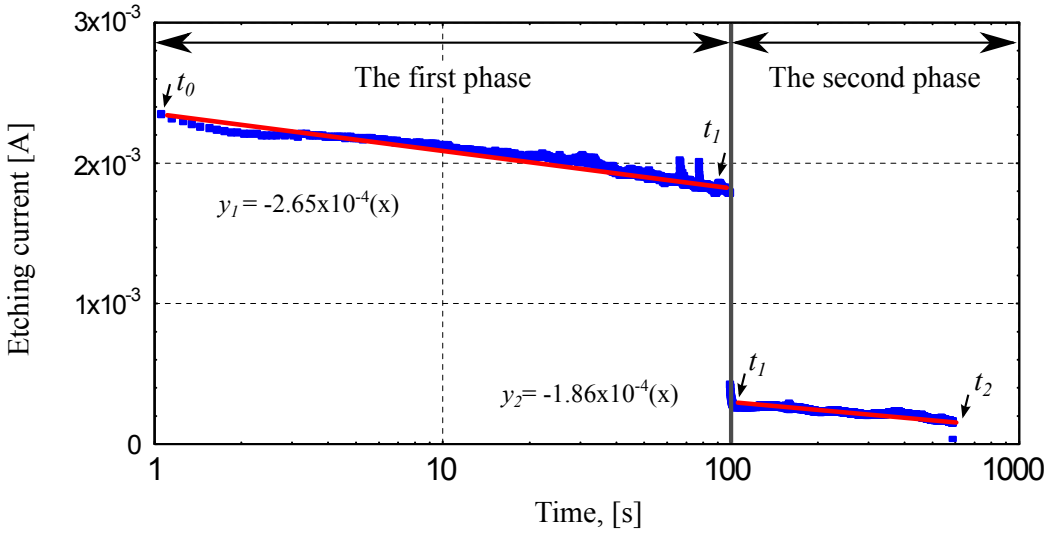

Fig. 5.3: Variation of the etching current as a function of etching time

performed until the wire is significantly constricted and thus prepared for the second phase. The slope of linear regression of the etching current can be seen in fig. 5.3, where the slope is equal to -2.65×10^{-4}. Consequently, we are able to estimate the drop off time from the initial current based on the result of linear regression. However this is not used for the first phase, since for two-phase etching, phase one is always terminated prematurely and continued in a different electrolyte as phase two. Thus this approach can only be used for single-phase etching. The current for the second phase can also be modelled using the linear regression function, where the slope for the 2nd phase equals -1.86×10^{-4} and continues until the bottom part drops off.

According to our experiments, there is a clear relation between the length of these two etching phases and the diameter of the etched wire in order to achieve the desired tip geometry and to avoid tip blunting. We named this ratio the phase-length ratio (PLR); it can be expressed with the help of fig. 5.3 as:

$$plr = \frac{t_1 - t_0}{t_2 - t_1}, \tag{5.1}$$

at $(0 < plr < 1)$, where t_0 is the initial etching current, t_1 is the current at the time of the second phase, and t_3 is the dropping-off time. Even though the PLR differs for different diameters of wire, the value of the 2nd differential gradient that is used to activate the gradient detector remains the same.

5.3 Characterization of the Prepared Field Emitter

The prepared sample of the experimental field-emitter was successfully tested in a vacuum chamber under HV vacuum conditions, at a pressure of 10^{-6} Pa. Since the structure is not homogeneous, each layer must be described in detail in order to obtain data important for improving the process. Fig. 5.4a. was obtained using classical SEM at 20 kV and shows the tip of the emission cathode.

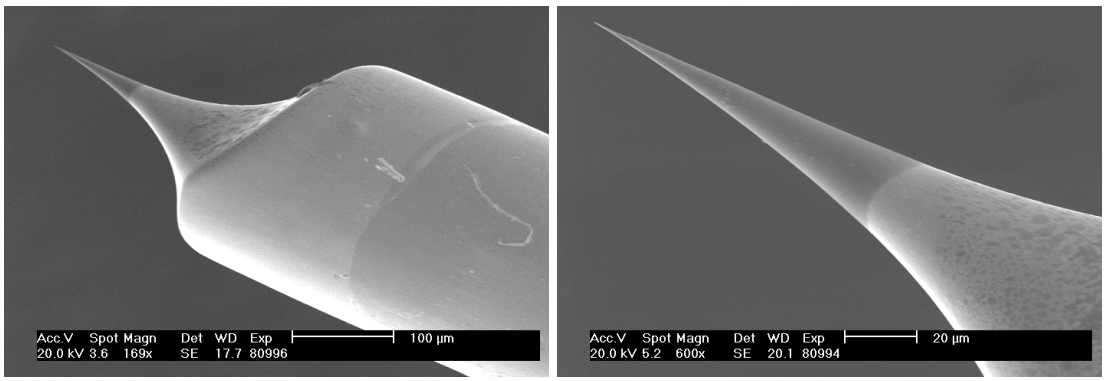

Fig. 5.4: SEM image of the a) tip of the cathode, b) surface covered by epoxy

From the results of the EDS analysis it can be seen that even though tungsten is predominant, there is a significant amount of contaminants present on the surface.

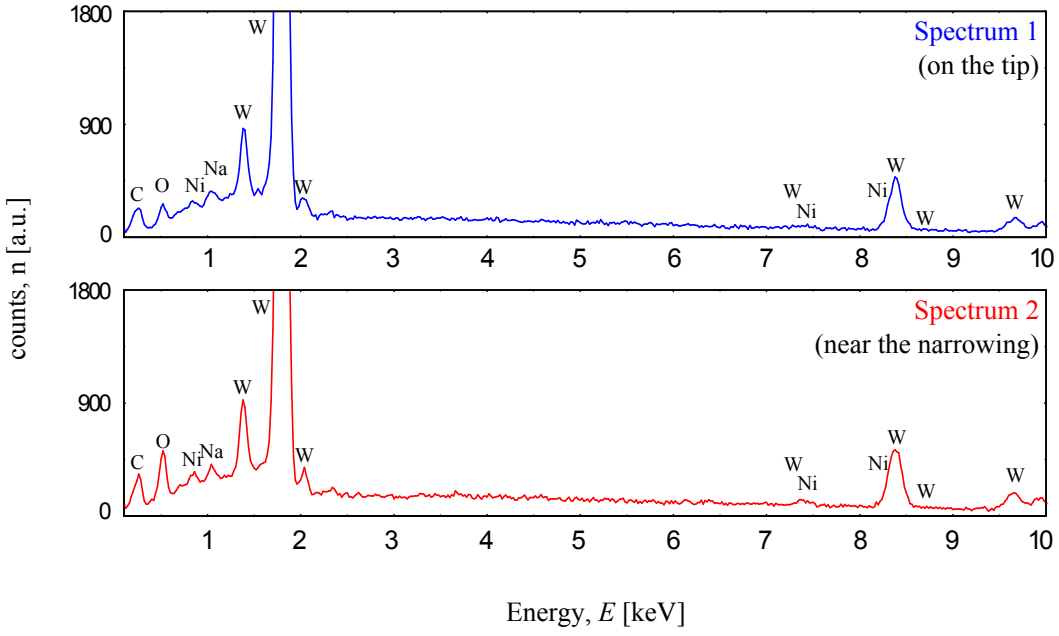

Fig. 5.5: Obtained spectra of the SEM-EDS analysis, a) EDS on the tip (blue), b) EDS in the area of wire narrowing (red)

The presence of carbon cannot be determined precisely since the method does not provide an accurate response, although it does give us information about its presence. The EDS spectrum was measured twice, first on the uncoated cathode tip and then near the region of the narrowing. Both measurements are comparable, which enables us to suggest further technology improvements.

From the first measurement, shown in fig. 5.5a., it can be seen that the tungsten is predominant although there is a significant amount of nickel and sodium, which originate from the etching process.

5.3.1 Characterization of the Epoxy Coating

As mentioned above, the epoxy coating is used in order to protect the tip against residual ions that are attracted to the tip, causing damage to it. In this section we will describe the physical and chemical properties of this coating, which is created at the end of the preparation process.

From the chemicals, the epoxy is based on Diglycidyl Ether of Bisphenol A, commonly abbreviated as DGEBA, with the molecular formula $C_{21}H_{24}O_4$. DGEBA is a chemical compound used as a constituent of epoxy resins. It is a derivative of bisphenol A that is used in epoxy resins for its cross-linking properties [55]. The commercial product used is Epoxylite 6001M (from The P.D. George Company).

As mentioned above, the epoxy layer is deposited by immersing the etched tip into the epoxy and cured in the temperature chamber in two phases. In the first phase, solvents present in the epoxy are evaporated. This phase takes approximately one hour, during which the is held at a temperature of 100 °C. In the second phase, the epoxy is cured at a temperature of 180 °C. During the second phase, the surface is fully hardened, and the epoxy layer becomes rigid and compact.

Circular samples were prepared in order to determine the dielectric constant, which was further calculated from the geometric capacity that is given by:

$$\epsilon_r = \frac{C}{C_0} = \frac{1.41 \times 10^{-11}}{2.48 \times 10^{-12}} = 5.67 \tag{5.2}$$

where $C_0 = \epsilon_0 S/d$, A is the area of the electrodes and d is the separation between the two electrodes.

5.4 Measurement Setup for Emission Properties

The multi-purpose measurement setup used for electrical, optical, and stability analysis is shown in fig. 5.6. The system is divided into three main parts: a vacuum chamber based on two-phase venting, a computer with instruments connected to it used to measure electrical parameters, and a CCD module, which enables the systém to capture incident electron beam patterns.

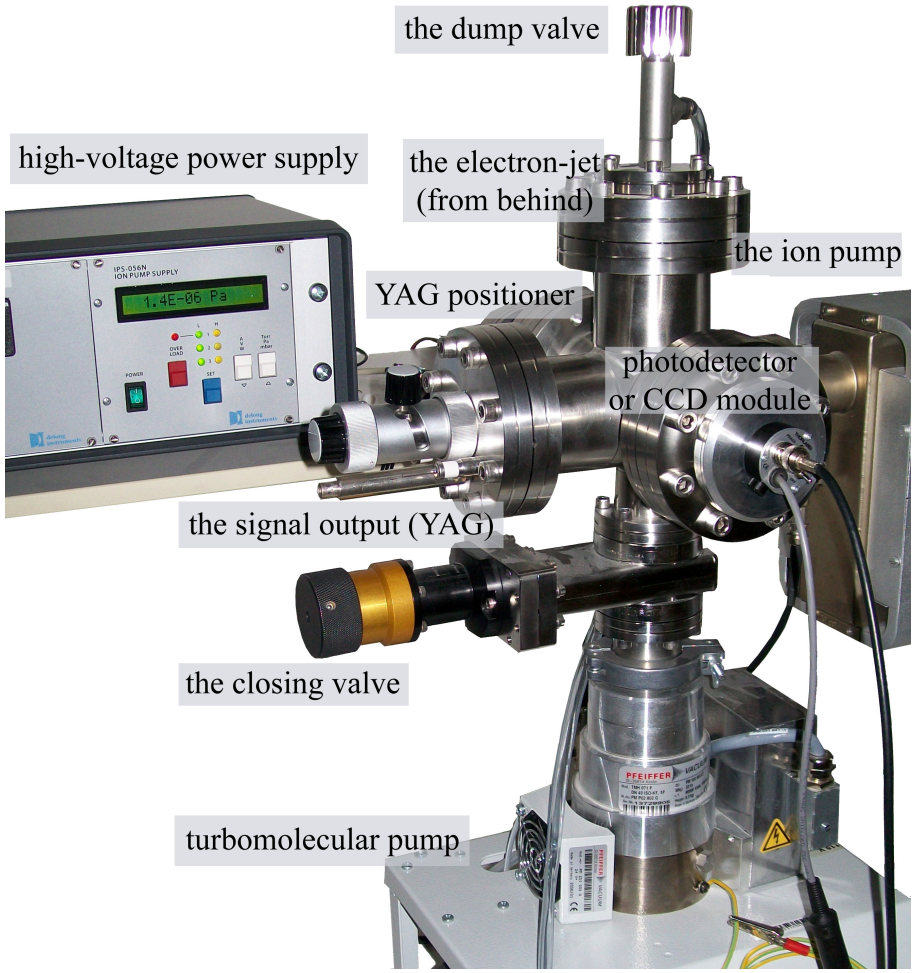

Fig. 5.6: The measurement setup including the high-voltage power supply.

The high vacuum is provided using the combination of a turbomolecular pump and an ion pump, enabling it to achieve a 10^{-6} Pa. The described setup is adapted to be used for two various modifications.

5.5 Fowler-Nordheim Analysis

The main goal of this section is to provide a physical characterization of the sample field-emitter whose preparation has been described above. For this reason, the Fowler-Nordheim analysis has been used. The objective is to show that the phenomenon of electrons moving through the vacuum of the experimental emitter is in fact an example of Fowler-Nordheim tunnelling, also known as quantum tunnelling. Using Fowler-Nordheim Analysis it is shown that the V-I relation is consistent with the expected tunnelling model.

Tab. 5.1: The tabulated experimental data for the F-N analysis

I [A]	V_{ext} [V]	$\ln(I/V^2)$ [A·V^{-2}]	$1/V_{ext}$ [V^{-1}]	F [V·m^{-1}]
1.46×10^{-6}	195	-23.98	5.13×10^{-3}	6.11×10^{9}
1.70×10^{-6}	200	-23.88	5.00×10^{-3}	6.26×10^{9}
2.40×10^{-6}	208	-23.62	4.81×10^{-3}	6.51×10^{9}
3.20×10^{-6}	215	-23.39	4.65×10^{-3}	6.73×10^{9}
3.60×10^{-6}	223	-23.35	4.48×10^{-3}	6.98×10^{9}
4.20×10^{-6}	224	-23.20	4.46×10^{-3}	7.01×10^{9}
4.40×10^{-6}	227	-23.18	4.41×10^{-3}	7.11×10^{9}
5.10×10^{-6}	234	-23.10	4.27×10^{-3}	7.33×10^{9}
6.50×10^{-6}	242	-22.92	4.13×10^{-3}	7.58×10^{9}
8.50×10^{-6}	248	-22.70	4.03×10^{-3}	7.76×10^{9}
9.02×10^{-6}	251	-22.67	3.98×10^{-3}	7.86×10^{9}
1.20×10^{-5}	262	-22.47	3.82×10^{-3}	8.20×10^{9}

Data was gathered by measuring the total-emission current on the YAG along with measuring the extraction voltage. For a given voltage, the corresponding output current was read using a precise Agilent 34410A multimeter. Graphing these data yields an exponentially increasing trend as illustrated in fig. 5.7.a.

In order to show that our data fits the Fowler-Nordheim relation, a least squares fit must be performed. The slope of a last squared fit and the y-intercept are given by the following equations, where N is the number of data points (twelve in this case).

Another quantity of interest is the electric field intensity at the cathode tip, since according to the Fowler-Nordheim theory, the electric field at the the tip apex reduces the width of the energy barrier that confines electrons to the interior of the cathode.To find the electric field strength, the field-voltage proportionality factor KR must be calculated, using an iterative numeric procedure described by Robert Gomer in 1961 [12].

Referring back to table 5.1, it can be seen that there is a clearly exponential increase of current as a function of voltage 5.7.a., which can be explained by quantum tunnel-

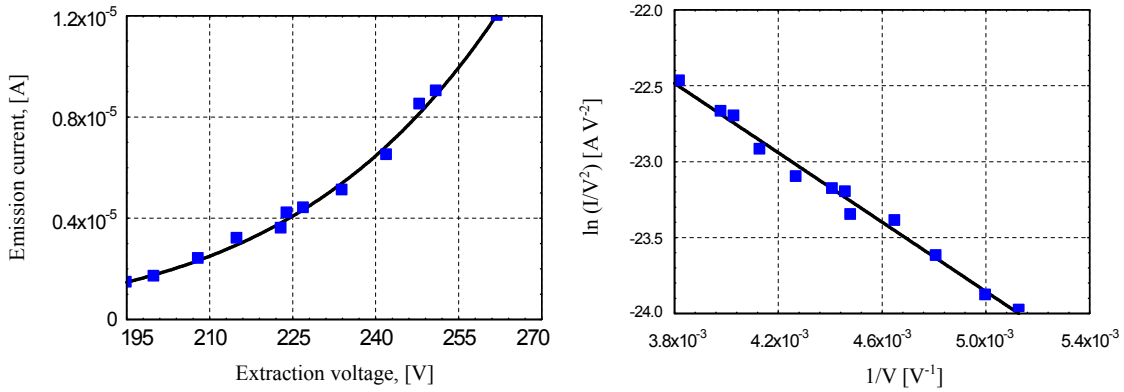

Fig. 5.7: a) Exponential dependence of current vs. extractor voltage, b) Linear dependence of data, after Fowler-Nordheim analysis

ling [9]. Based on the analysis of $(1/V)$ against the $\ln(I/V^2)$, as seen on fig. 5.7.b., apparently linear relation was yielded. The linearity of this relation provides the essential physical phenomenon of the experiment. The results achieved are illustrated by the following table.

Tab. 5.2: Calculated data

FN slope	FN intercept	KR / m	A_e / m^2	j_{260V} / A m^{-2}	F_m / V m^{-2}
-1.15×10^3	-18.12	3.19×10^{-8}	6.48×10^{-18}	1.85×10^{12}	7.1×10^9

5.6 Band Diagram of the Sample Cathode

As was mentioned previously, atomically clear surfaces cannot be expected on real emitters, since a thin oxide layer develops very quickly, and its presence is thus unavoidable. But even though the presence of the oxide layer can decrease the emitter's emissions, it can also protect them against degradation. For a clean metallic surface, the field emission density can be calculated using the Fowler-Nordheim equation. Therefore, we are working with a three-layer composite structure represented by a metal-oxide-epoxy interface with various parameters of each component. Tungsten acts here as a metal; tungsten trioxide is used as an oxide layer. The epoxy coating affects the emission current by limiting the supply of carriers to the surface, which is strictly dependent on the applied potential.

From the previous analysis [16] it can be seen than the tungsten-oxide layer acts as a semiconductor of some type that we should further specify, and therefore it has an

essential influence on the stability of the emission current and involves noise mechanisms typical for semiconductor devices. With knowledge of tungsten trioxide electron affinity χ (3.33 eV) and energy gap E_g (2.8 eV), it is possible to determine the difference between the energy of the vacuum level E_a and the energy of the valence band E_v, which can be calculated as a sum of the oxide electron affinity and it's energy band, yielding the value of energy 6.13 eV. Upon estimating the value of the work function from the calculated energy level, we obtain the ionization level for our type of semiconductor. The value obtained is about 0.53 eV, that is, much less than half of the energy band (1.4 eV). Therefore, it can be concluded that our semiconductor has p-type conductivity.

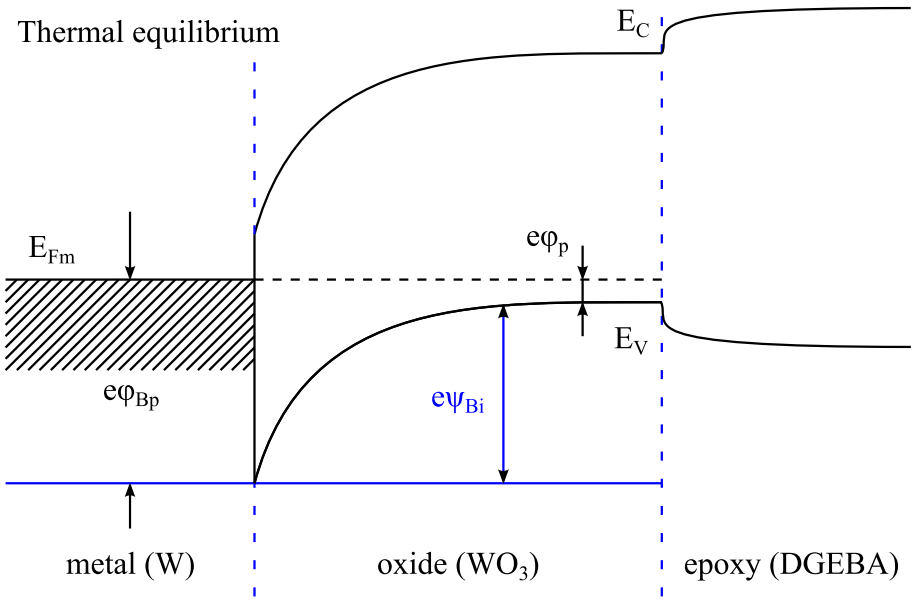

Fig. 5.8: Band structure of ultra sharp tungsten field emitter covered by thin oxide and epoxy layer at thermal equilibrium, without applied electric field

For an oxide-epoxy-covered surface without an applied electric field, the emitter can be modelled using two one-dimensional barriers divided into three parts, as illustrated in fig. 5.3. In a metal-oxide system, the barrier height is simply the difference between the metal's work function and the electron affinity of the semiconductor. On the contrary, for ideal contact between a metal and a p-type semiconductor, the barrier height $e\varphi_{Bp}$ is given by eq.5.3, [13]:

$$e\varphi_{Bp} = E_g - e(\varphi_m - \chi), \tag{5.3}$$

where $e\varphi$ is the electron affinity of semiconductor. Fig. 5.8 also illustrates the values of the oxide surface potential $e\psi_{Bi}$ and the ionization potential $e\varphi_p$. By increasing the

extraction voltage in the case of reverse bias 5.9 the value of potential barrier is raised up to $e\psi_{Bi} + eV_R$, and therefore the value of the current density can be written as [13]:

$$J = J_s \left(e^{\frac{-eV_R}{kT}} - 1 \right). \tag{5.4}$$

Regarding the epoxy layer, the interface properties between metal and polymers are generally not very well understood, since these materials are of entirely different characters. However, a recent study reported the presence of an image force lowering the potential barrier at the metal-semiconductor polymer [20]. Based on this effect, information on the polymer's electrical properties can be obtained. Because of the relative permittivity (ϵ_r) the slope of the oxide barrier is lowered to $1/\epsilon_r$ times that of the vacuum barrier. Additional lowering of the barrier is caused by the effect of image charge, for which stands that $e^2/16\pi\epsilon_0\epsilon_r z$. Thus the barrier can be expressed as [27]:

$$U(z) = \begin{cases} E_F + E_B - \frac{e^2}{16\pi\epsilon_0\epsilon_r z} - \frac{eFz}{\epsilon_r} & (0 < z < t_{ox}) \\ E_F + \varphi - \frac{e^2}{16\pi\epsilon_0 z} - eFz & (z > t_{ox}) \\ 0 & (z < 0) \end{cases} \tag{5.5}$$

where E_F stands for Fermi level of the metal, E_B the oxide barrier height, F the intensity of the applied electric field, φ the work function of the metal, and t_{ox} stands for the thickness of the oxide film. The emission current density can be in general written as it was mentioned in Hawkes and Kasper [13]

$$J(F,T) = e \int_0^\infty N(W,T) D(F,W,T) dW, \tag{5.6}$$

where $N(W,T)$ stands for electron density with kinetic energy W at temperature T and $D(F,W,T)$ is the tunnelling probability, which can be written as follows [27].

$$N(W,T) = \frac{m' k_B T}{2\pi^2\hbar^3} \ln\left[1 + e^{-\frac{W-E_F}{kT}}\right], \tag{5.7}$$

Therefore, for the whole function we can write

$$N(W,T) = \begin{cases} \frac{m' k_B T}{2\pi^2\hbar^3} \ln\left[1 + e^{-\frac{W-E_F}{kT}}\right] & (E > E_C, E < E_V) \\ 0 & (E_V < E < E_C) \end{cases}, \tag{5.8}$$

where m' is the effective mass of electron in the emitter material.

Based on previous calculations, it is evident that the density of the emission current decreases as the width of the oxide layer increases. When it reaches its minimum, the trend reverses and tends to slowly increase until it reaches the saturation level. As you can see in the fig. 5.9, the barrier area of the oxide increases as the oxide layer increases,

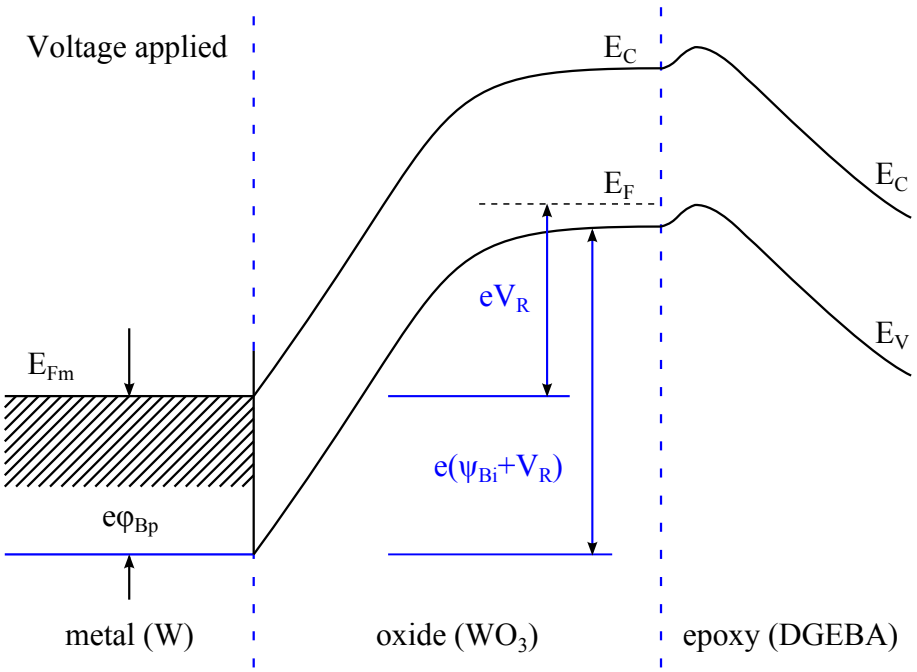

Fig. 5.9: Band structure of an ultra-sharp tungsten field emitter, covered in a thin oxide and epoxy layer (reversed bias applied).

while the energy level is lowered. As a result, the increase of the oxide layer thickness alters the oxide part of the barrier to increase more than vacuum part is decreased.

On the basis of our calculations, it can be concluded that there is a significant difference between the clean (virgin) emitter and the oxide-covered one. The emission's saturation level is reached when the emission current leaks through the oxide layer, causing the vacuum part of the barrier to stop altering the emission current.

5.7 Finite Element Modelling using Comsol

Using *Comsol Multiphysics 4.2a*, finite element simulations were performed in order to calculate those physical quantities whose exact determination is based on solving very complicated partial-differential equations (PDE).

Fig. 5.10 illustrates the potential distribution near the surface of the experimental emitter. According to our expectations, it can be seen that the highest field gradient occurs near the cathode surface, especially around the tip. This makes it possible to achieve a field intensity of the strength needed in order to emit electrons. For a tip with a tip diameter of 50 nm, at an extraction voltage of 200 V, the field strength near the cathode tip is approximately 6.32×10^9 V/m which corresponds with the results obtained by experimental Fowler-Nordheim analysis stated above.

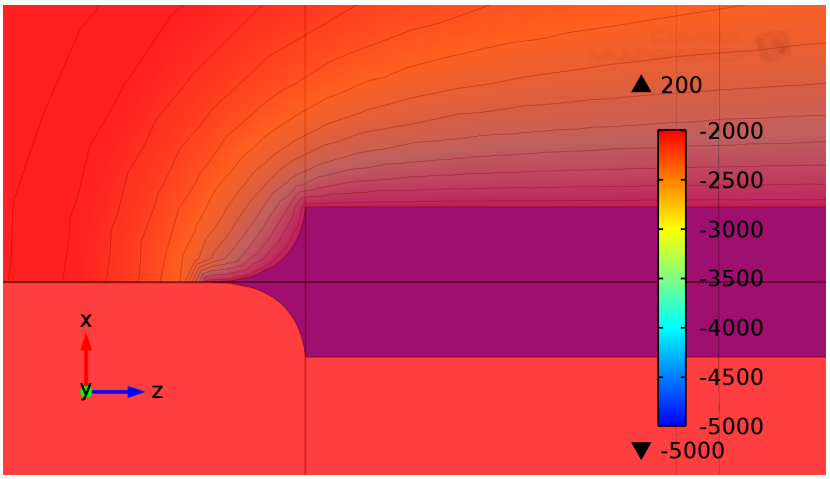

Fig. 5.10: Visualisation of the electric potential distribution near the tip of the cathode

Figure (5.11) illustrates the lines of force between the extraction electrode and the cathode the (blue lines). It can clearly be seen here how the lines of force are bent towards the aperture in the extraction electrode. The exact positioning of the lines of force depends on several factors. In the ideal situation, the factors influencing the distribution are: the extractor-voltage, the radius of the cathode tip, the aperture in the extractor electrode, and the separation between the extractor electrode and the cathode.

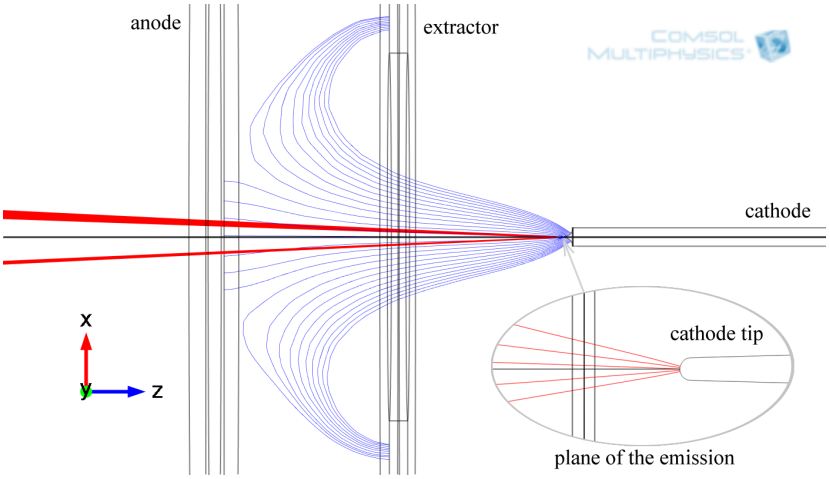

Fig. 5.11: Particle tracing and force-lines of the field visualisation

The fig. 5.11 also shows the approximate electron trajectory of the electrons (red line) that are emitted from the region where the local electric field is stronger than 1×10^9 V/m, which is considered to be the theoretical threshold level for the field emission of electrons into vacuum.

5.8 Results of the Noise Analysis

The noise is strongly affected by the work regime of the cathode. In the saturated regime (i.e. in the regime, where additional increase of voltage does not further increase current) the stability is higher, since the current stability is indirectly proportional to the amount of charge carriers. According to our measurements, the saturated regime is located > 300 V of extraction voltage, where the further increase of voltage does not further affect the noise level.

Above all, the quality of used materials has significant impact on the stability of electron emission. From the technological point of view, the biggest problem poses the presence of impurities atoms contained inside the polycrystalline wire of tungsten, that locally affects the work function. The work function modulation of electron emission plays important role in the flicker part of noise spectrum. The flicker part of the spectra are to be described by $1/f$, $1/f^{3/2}$, $1/f^2$ type spectral functions. While the beam of primary electron would induce shot noise, additional flicker-like contribution is possible on the spectra of the work function fluctuations, which is characteristic for the field emission in general.

The flicker noise proved to be dependent on the residual gas coverage, where the $1/f$ part is enlarged on the account of the shot noise. The $1/f$ spectrum of gaseous adsorbate can be described by the adsorption-desorption model [15], [23] using the flicker noise interpretation described by Schottky [21] with an appropriate distribution of time constants. The surface migration of adsorbate should play an important role as well, since the fast hopping process on the surface might be responsible for the noise observed over the analysed frequency range.

The ion bombardment of residual gasses causes spatial changes in the surface topography, especially to the epoxy layer which further affects geometry of the electric field and thus affects the emission stability and decreases the current density. Decrease of the current density might be also influenced by the strong electric field on the tip of the cathode, which (along with the Joule heat caused by passing electrons) deforms the crystalline structure of the emission plane and thus decreasing the level of the intensity of applied electric field. Level of the thermal noise induced by the Joule heat can be easily calculated from the knowledge of resistance of the cathode expressed mathematically as $4\mathrm{k}TR$.

Generation-recombination noise proved to be caused by the emission-capture process, which takes place on the surface of the cathode. Using the probability model based on Kolmogorov equations, it was show that the probability of particle capture on the surface of the cathode is proportional to the captured particle velocity and surface site cross section. The derived probability distributions are similar to the Fermi-Dirac statistics known from semiconductor physics.

6 CONCLUSIONS AND CONTRIBUTIONS OF THE WORK

In accord with theory, it has been proven that to achieve a high-quality cold field-emitter, a metal with specific properties must be used. The most important of these are a low work function and a high melting point. Based on the conditions stated above, the following transition metals meet the requirements: Tungsten (W), Hafnium (Hf), Tantalum (Ta), Niobium (Nb), and Lanthanum (La). The experiments conducted over the course of this thesis work were all carried out on tungsten. In order to describe the experimental emitter, a band diagram describing the metal-oxide-epoxy junction was solved. The theoretical expectations were verified practically, using the experimental cathode in a high-vacuum chamber at 10^{-6} Pa.

In the experimental portion of this work, a method for preparing a metal-oxide-epoxy cathode was devised. Within the method devised, the cathode tips were prepared using electrochemical etching of tungsten. The oxide layer on the surface was prepared using anodic oxidation, and lastly, the oxidized tips were covered in a thin layer of epoxy that has been polymerized in a thermal chamber. Only cathodes of a sufficiently thin tip diameter (< 100 nm) are suitable to be used within the cold field-emission-based jet. Theoretically, the performance of the cathode could be improved by reducing the tip diameter of the cathode, which should be as small as possible (only a few atoms in the optimal case).

It has been determined that the diameter of the tip has a fundamental impact on the electric field gradient. Mathematically, the function can be described by the mutual ratio of the local electric field (the electric field on the tip) and the macroscopic electric field (the axial electric field). The cathode's lifetime was one of the examined properties. It has been discovered that there is a direct proportion between the noise of the cathode's emission current. The most important mechanism causing the unwanted noise is the generation-recombination (G-R) process, which originates from the superposition of several $1/f$ noise mechanisms.

The topic covered by this thesis has been published in number of scientific articles: **5** local **conference** papers, **6 international conference** papers (1 of these papers is registered in **Scopus** ©), **3 reviewed journal** papers, and **2 impacted** journal papers (one paper is currently available through **Scopus** ©, and one is still **in press**).

To summarize, the main contribution of the work can be summarized in three main points:

1 Development of a preparation methodology for composite ultra-sharp field-emission cathodes,
2 Implementation of this methodology and of an experimental design for an automated etching setup (hardware and software intended for sample preparation), and lastly a
3 Proposal for a characterization methodology based on the Fowler-Nordheim analysis, the FEM simulation (COMSOL) and the Noise Spectroscopy method.

BIBLIOGRAPHY

[1] BUSCH, H. Berechnung der Bahn von Kathodenstrahlen im axialsymmetrischen elektromagnetischen Felde [Calculating the path of cathode trajectories in axisymmetric electromagnetic field]. *Annalen der Physik*. 1926, vol. 386, iss. 25, p. 974-993. ISSN 00033804. DOI: 10.1002/andp.19263862507.

[2] CREWE, A. V. A High-Resolution Scanning Transmission Electron Microscope. *Journal of Applied Physics*. 1968, vol. 39, iss. 13, p. 5861. ISSN 00218979. DOI: 10.1063/1.1656079.

[3] CREWE, A. V. and J. WALL. A scanning microscope with 5 Å resolution? *Journal of Molecular Biology*. 1970-03-28, vol. 48, iss. 3, p. 375-393. ISSN 00222836. DOI: 10.1016/0022-2836(70)90052-5.

[4] DELONG, A. et al. Rastrovací elektronový mikroskop s autoemisní tryskou [Scanning electron microscope with a cold field-emission jet]. *Slaboproudý obzor*. 1978, vol. 39, iss. 443.

[5] DJUBUA, B. C. and N. N. CHUBUN. Emission properties of Spindt-type cold cathodes with different emission cone material. *IEEE Transactions on Electron Devices*. 1991, vol. 38, iss. 10, p. 2314-2316. ISSN 00189383. DOI: 10.1109/16.88516.

[6] DUTTA, P. and P. HORN. Low-frequency fluctuations in solids: 1/f noise. *Reviews of Modern Physics*. 1981, vol. 53, iss. 3, p. 497-516. ISSN 0034-6861. DOI: 10.1103/RevModPhys.53.497.

[7] ECKERTOVÁ, L. and L. FRANK. *Metody analýzy povrchů: elektronová mikroskopie a difrakce* [*Methods of surface analysis: electron microscopy and diffraction*]. 1. ed. Prague: Academia, 1996, 379 p. ISBN 80-200-0329-0.

[8] MARTIN, E. E., J. K. TROLAN and W. P. DYKE. Stable, High Density Field Emission Cold Cathode. *Journal of Applied Physics*. 1960, vol. 31, iss. 5, p. 782. ISSN 00218979. DOI: 10.1063/1.1735699.

[9] FOWLER, R. H. and L. NORDHEIM. *Proc. Roy. Soc. (London) A*, 119(781):173, 1928.

[10] FRANSEN, M. J. *Towards high-brightness, monochromatic electron sources.* [S.I.: s.n.], 1999. ISBN 90-901-2398-9. PhD. thesis. Delft University of Technology.

[11] GOLUBEV, O. L. and V. N. SHREDNIK. Heat-field treatment of tips made of tungsten-hafnium alloy. *Technical Physics*. 2003, vol. 48, iss. 6, p. 776-779. ISSN 1063-7842. DOI: 10.1134/1.1583834.

[12] GOMER, R. *Field Emission and Field Ionization*, Harvard University Press, 1961, p. 47. Reprinted in 1993 (American Vacuum Society Classic Series, Number 1-56396-124-5).

[13] HAWKES, P. W. and E. KASPER. *Electron optics*. 2. Engl. ed., rev. Oxford: Pergamon Pr, 1972. ISBN 978-008-0162-287.

[14] HIBI, T. High-Resolution Replicas and Their Application. *Journal of Applied Physics*. 1954, vol. 25, iss. 6, p. 712. ISSN 00218979. DOI: 10.1063/1.1721721.

[15] KLEINT, C. *Ann. Phys.* (Leipzig) 10 (1963) 295, 309.

[16] KNAPEK, A. et al. Cold field-emission cathode noise analysis. *METROL MEAS SYST*. 2012, vol. 2012, iss. 2, p. 417-422. ISSN 0860-8229.

[17] DYKE, W. P. et al. Electrical Stability and Life of the Heated Field Emission Cathode. *Journal of Applied Physics*. 1960, vol. 31, iss. 5, p. 790. ISSN 00218979. DOI: 10.1063/1.1735700.

[18] MELMED, A. J. The art and science and other aspects of making sharp tips. *Journal of Vacuum Science*. 1991, vol. 9, iss. 2, p. 601. ISSN 0734211x. DOI: 10.1116/1.585467.

[19] PETERS, J. et al. Erosion mechanisms of hafnium cathodes at high current. *Journal of Physics D: Applied Physics*. 2005-06-07, vol. 38, iss. 11, p. 1781-1794. ISSN 0022-3727. DOI: 10.1088/0022-3727/38/11/019.

[20] RIKKEN, G. et al. Schottky effect at a metal-polymer interface. *Applied Physics Letters*. 1994, vol. 65, iss. 2, p. 219-. ISSN 00036951. DOI: 10.1063/1.112678.

[21] SCHOTTKY, W. *Phys. Rev. 28* (1926) p. 74.

[22] SIKULA, J. and M. LEVINSHTEIN. *Advanced experimental methods for noise research in nanoscale electronic devices*. Boston: Kluwer Academic Publishers, 2004, p. 271-278. ISBN 14-020-2170-4.

[23] TALBOT, J., G. TARJUS and P. VIOT. Adsorption-desorption model and its application to vibrated granular materials. *Physical Review E*. 2000, vol. 61, iss. 5, p. 5429-5438. ISSN 1063-651x. DOI: 10.1103/PhysRevE.61.5429.

[24] VAN OOSTROM, A. Temperature dependence of the work function of single crystal planes of tungsten in the range 78 - 293K. *Physics Letters*. 1963, vol. 4, iss. 1, p. 34-36. ISSN 00319163. DOI: 10.1016/0031-9163(63)90576-6.

[25] WOOD, R. W. New Form of Cathode Discharge and the Production of X-Rays, together with Some Notes on Diffraction. Preliminary Communication. *Physical Review (Series I)*. 1897, vol. 5, iss. 1, p. 1-10. ISSN 1536-6065. DOI: 10.1103/PhysRevSeriesI.5.1.

[26] XU, N. S. and E. S. HUQ. Novel cold cathode materials and applications. *Materials Science and Engineering: R: Reports*. 2005, vol. 48, 2-5, p. 47-189. ISSN 0927796x. DOI: 10.1016/j.mser.2004.12.001.

[27] YANG, G. and K. K. CHIN. Electron field emission through a very thin oxide layer. *IEEE Transactions on Electron Devices*. 1991, vol. 38, iss. 10, p. 2373-2376. ISSN 00189383. DOI: 10.1109/16.88528.

Ing. Alexandr Knápek

Contact Information

Brno University of Technology
Department of Physics, FEEC
Technická 8, 616 00 Czech Republic

Phone: +420 54114 3257
E-mail: xknape03@stud.feec.vutbr.cz

Current Occupation

PhD. student at Brno University of Technology, Department of Physics, FEEC.
Sep. 2009 - April 2013 (expected)

Employee at Institute of Scientific Instrument of the ASCR
Oct. 2012 - present

Education

Brno University of Technology, Brno, Czech Republic

Master's degree, Faculty of Electrical Engineering and Communication,
Telecommunication and Information Technics (09/2006 - 06/2008)

Bachelor's degree, Faculty of Electrical Engineering and Communication,
Teleinformatics (09/2003 - 06/2006)

Projects

Principal investigator:

Research of methods, intended for increasing the quality of the optoelectronic material and components, 01/2010 - 12/2010

Co-investigator:

Defect diagnostics of the materials for electronics,
01/2011 - 12/2014 (expected)

Design and innovation of the measurement system for the dielectric measurements,
01/2010 - 12/2010

Important Publications

KNÁPEK, A., GRMELA, L., ŠIKULA, J. and O., ŠIK. Cold field-emission cathode noise analysis. *METROL MEAS SYST*, **2012, vol. 2012, no. 2, p. 417-422. ISSN: 0860-8229. (IF = 0.764)**

KNÁPEK, A. and L., GRMELA. Fabrication technology of the cold field-emission cathodes based on tunsten with epoxy coating. *CHEM LISTY*, **2013 (in print). ISSN: 1213-7103, (IF = 0.529)**

KNÁPEK, A., GRMELA, L., ŠIKULA, J., HOLCMAN, V. and A., DELONG. Noise of Cold Emission Cathode. In *ICNF2011: 2011 21st International Conference on Noise and Fluctuations*. **Toronto, Canada: IEEE, 2011. p. 84-87. ISBN: 978-1-4577-0191-7.**

KNÁPEK, A. and L., GRMELA. *Stability Analysis of Cold- Emission Cathodes with Epoxy Coating*. *ElectroScope*, **2011, vol. 2011, no. 2, p. 1-5. ISSN: 1802-4564.**

KNÁPEK, A., KRČÁL, O. and L., GRMELA, L. Schottky Nano-Tip Cathodes Fabrication and Diagnostics. *ElectroScope*, **2010, vol. 2010, no. 1, p. 1-4. ISSN: 1802-4564.**

ABSTRACT

This PhD thesis describes, and covers the preparation of field-emission cathodes that represent a high-quality, inexpensive source of electrons for devices that work with a focused electron beam. In this work, an improved method of electrochemical fabrication is used for the preparation of a composite field-emission cathode. The composite structure improves current stability in comparison to tungesten-based pure field-emission cathodes. Improvements to the technology used were implemented on the basis of findings obtained using spectrum noise diagnostics, which are based on measuring and evaluating the emission current in the time and in frequency domains. Additionally, noise spectroscopy provides important information about charge transport, electron mobility, and lifespan, which is essential for future research. Results obtained using the experimental method have been further supplemented with theoretical data provided by a computer simulation in order to establish characterization procedures for improved field-emission cathodes.

ABSTRAKT

Téma doktorské práce se zabývá přípravou a popisem katod na bázi studené polní emise, jenž představují kvalitní a levný elektronový zdroj pro zařízení pracující se zaostřeným elektronovým svazkem. Pro přípravu kompozitní autoemisní katody byla využita elektrochemická metoda výroby. Kompozitní struktura katody zlepšuje proudovou stabilitu ve srovnání s čistě autoemisními katodami na bázi wolframu. Na základě charakterizace katody, jenž byla nově provedena metodou šumové spektroskopie, byla implementována technologická zlepšení stávající výroby. Metoda šumové spektroskopie je založena na analýze emisního proudu v časové a kmitočtové rovině, ale především poskytuje informace o nosiči náboje, o jeho pohyblivosti a dále o životnosti katody. Výsledky experimentální části byly rozšířeny teoretickými simulacemi, vedoucími k návrhu metodiky charakterizace vylepšené autoemisní katody.

KNÁPEK, Alexandr *Methods of Preparation and Characterisation of Experimental Field-Emission Cathodes*: doctoral thesis. Brno: Brno University of Technology, Faculty of Electrical Engineering and Communication, Department of Physics, 2013. 31 p. Supervised by Prof. Ing. Lubomír Grmela, CSc.